



CFD study on the influence of turbulence promoter configurations on flow patterns in tubular membrane channel

Yuanfa Liu^{a,*}, Yanfen Li^a, Jun Zhang^a, Gaohong He^b, Chao Huang^a, Shugang Xu^a

^a*School of Textile and Material Engineering, Dalian Polytechnic University, Dalian, China, email: Liuyf@dipu.edu.cn (Y. Liu), 158516278@qq.com (Y. Li), 844588135@qq.com (J. Zhang), 599003686@qq.com (C. Huang), 1339552526@qq.com (S. Xu)*

^b*School of Chemical Engineering, Dalian University of Technology, Dalian, China, email: hgaohong@dlut.edu.cn*

Received 1 July 2018; Accepted 12 December 2018

ABSTRACT

A computational fluid dynamics (CFD) study was conducted to simulate the turbulent flow in the tubular channel centrally inserted with different types of turbulence promoters, that is, rod baffle, disc baffle and helical baffle, respectively. The main purpose of this study is to numerically investigate the influences of turbulence promoter configurations on flow patterns, behaviors and feature within membrane modules. Simulation results show that the disc baffle generates a rather more complex flow fields within membrane module than helical baffle or rod baffle, thereby causing the more intense fluctuations of crossflow velocity or wall shear stress and producing the fairly higher turbulence level of fluid flow. It indicates that the disc baffle can achieve a better membrane performance than helical baffle or rod baffle. The experimental result of microfiltration of calcium carbonate suspension is consistent with the prediction of CFD simulation. However, the pressure drop along the channel is significantly increased due to the presence of turbulence promoter, resulting in the high energy consumption of membrane modules. Therefore, the optimization of baffled membrane system involves a trade-off between these competing effects

Keywords: CFD; Membrane fouling; Turbulence promoter; Flux enhancement

1. Introduction

The performance of microfiltration process is severely hindered by the phenomenon of membrane fouling, that is, deposition of rejected particles on membrane surfaces, leading to the blockage of membrane pores [1] or formation of a cake layer [2]. Membrane fouling is regarded as the major reason accounting for the undesirable decline of permeate flux [3], which restricts membrane module productivity. To alleviate the adverse effects of membrane fouling, turbulence promoters are widely utilized in the crossflow membrane filtration processes. The use of turbulence promoters can significantly improve the hydrodynamic condition on the membrane surface and thus enhance the filtration performance. To clearly understand the enhancement mechanism by turbulence promoters, it is

necessary to analyze the hydrodynamic characteristics inside the membrane modules.

Computational fluid dynamics (CFD) is a useful tool to investigate the process involved with fluid flow because it can provide a lot of interesting information about flow fields without recourse to costly experimental work. Increasingly more researchers utilized CFD technique to gain insight into the phenomena taking place within membrane modules during various processes including microfiltration [4], ultrafiltration [5], nanofiltration [6], reverse osmosis [7], pervaporation [8], gas separation [9], membrane bioreactor [10], membrane distillation [11], membrane contactor [12] and membrane reactor [13]. In addition, there also is a large amount of literature related to CFD simulation of turbulence promoter-assisted membrane systems. Liu et al. [14] conducted CFD studies on the performance of microfiltration

* Corresponding author.

enhanced by a helical screw insert, and found that the hydrodynamics of fluid flow in the membrane tube was entirely changed. The rotational flow pattern could increase the scouring effect on the tube wall, thereby reducing the particle deposition on membrane surfaces and improving the filtration performance. Koutsou et al. [15] numerically simulated the fluid flow in a plane-channel containing a periodic array of cylindrical turbulence promoters. Through CFD simulation, they better understood the flow behavior, dominant features and structures, as well as the statistical characteristics. Liu et al. [16] carried out a CFD simulation for the baffle-filled membrane system and found that the presence of an array of central baffles or wall baffles caused remarkable increase of the average velocity and shear stress on the tube wall, which was responsible for the improvement of filtration performance. Cao et al. [17] simulated the flow patterns in a spacer-filled channel and found that both high shear stress regions and eddies were presented in the channel due to the spacer. The mass transfer enhancement on the membrane surface was directly related to the high shear stress value, velocity fluctuation and eddy formation. Shakaib et al. [18] conducted the three-dimensional CFD simulation for spacer-obstructed feed channels of membrane modules. They found the velocity profiles and average shear stress values significantly depended on the geometric parameters of parallel type spacers. Liu et al. [19] numerically investigated the influence of baffle arrangements on the flow patterns and found that baffle combination (combined use of central baffle and wall baffle) generated a rather more complex flow fields within membrane module than single type of baffle. It indicated that baffle combination could achieve better membrane filtration performance than wall baffle or central baffle. Santos et al. [20] simulated the flow patterns in membrane module filled with flow-aligned spacers, and found that the presence of spacers had a significantly influence on the flow structure in the channel.

By far, different types of turbulence promoters including disc baffle [21], static mixer [22], static rod [23], twisted wire-rod [24] and helical baffle [25], have been developed in various membrane processes. The use of turbulence promoters can effectively enhance the filtration performance due to the improved hydrodynamic conditions on the membrane surface. The turbulence promoter configuration plays a significant role in flow patterns and behaviors within membrane modules which greatly influences the membrane filtration performance. Experimental researches about the influences of turbulence promoter on the membrane performance have been extensively reported [26–30]. However, to the best of our knowledge, CFD study about the effects of turbulence promoter configurations on the flow patterns within membrane modules has been rarely reported.

In this study, the turbulent flow in tubular channel centrally inserted with a turbulence promoter (rod baffle, disc baffle or helical baffle) was numerically simulated to investigate the influence of turbulence promoter configurations on the hydrodynamic characteristics within membrane modules. The velocity vectors, velocity contours, distributions of wall velocity or wall shear stress, turbulent characteristics, pressure loss along the channel and mass transfer on the membrane surface were discussed for three baffle cases, respectively.

2. Numerical method

2.1. Model geometry

The simulated flow domain is a tubular channel of 15 mm in diameter and 70 mm in length where the turbulence promoter is centrally inserted. Three types of turbulence promoters are used in this study, that is, rod baffle, disc baffle and helical baffle, and their configurations are illustrated in Fig. 1. The insertion of rod baffle (10 mm in diameter and 50 mm in length) in the tubular channel produces a radial clearance gap of 2.5 mm between rod baffle and channel wall. Disc baffles (13 mm in diameter and 45 mm in length) are centrally mounted on a rod of 3 mm in diameter. The baffle interval is 10 mm and baffle thickness is 1 mm. The geometrical parameters of helical baffle (50 mm in length) are shown Fig. 1(c). For three baffle cases, the entrance length (distance between tube inlet and turbulence promoter) is 10 mm.

2.2. Governing equations

The fluid is assumed to be Newtonian and incompressible, and governed by the continuity and Navier–Stokes equations. To facilitate computational solution, the time-averaged method is extensively adopted in literature. Then the time-averaged continuity and Navier–Stokes equations (Reynolds equations) are obtained as follows.

$$\frac{\partial \rho}{\partial t} + \frac{\partial}{\partial x_i} (\rho u_i) = 0 \quad (1)$$

$$\frac{\partial \rho u_i}{\partial t} + \frac{\partial}{\partial x_j} (\rho u_i u_j) = \frac{\partial}{\partial x_j} \left[\mu \left(\frac{\partial u_i}{\partial x_j} + \frac{\partial u_j}{\partial x_i} \right) - \left(\frac{2}{3} \mu \frac{\partial u_i}{\partial x_i} \right) \right] - \frac{\partial p}{\partial x_i} + \frac{\partial}{\partial x_j} \langle -\rho u_i' u_j' \rangle \quad (2)$$

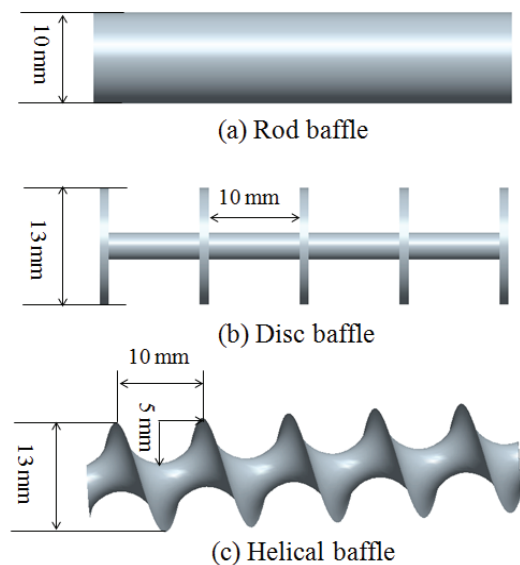


Fig. 1. Configurations of different turbulence promoters. (a) Rod baffle, (b) disc baffle and (c) helical baffle.

2.3. Turbulence model

The Re-Normalisation Group (RNG) $k-\epsilon$ model is employed to numerically simulate the turbulent flow in the turbulence promoter-inserted tubular channel since it is widely applied for the rotating and swirling flows. According to the RNG $k-\epsilon$ model, the turbulent kinetic energy k and turbulent dissipation rate ϵ are determined by the following equations.

$$\frac{\partial(\rho k)}{\partial t} + \frac{\partial(\rho k u_i)}{\partial x_i} = \frac{\partial}{\partial x_j} \left(\alpha_k \mu_{\text{eff}} \frac{\partial k}{\partial x_j} \right) + G_k + G_b - \rho \epsilon - Y_M + S_k \quad (3)$$

$$\begin{aligned} \frac{\partial(\rho \epsilon)}{\partial t} + \frac{\partial(\rho \epsilon u_i)}{\partial x_i} = & \frac{\partial}{\partial x_j} \left(\alpha_\epsilon \mu_{\text{eff}} \frac{\partial \epsilon}{\partial x_j} \right) + C_{1\epsilon} \frac{\epsilon}{k} (G_k + C_{3\epsilon} G_b) \\ & - C_{2\epsilon} \rho \frac{\epsilon^2}{k} - R_\epsilon + S_\epsilon \end{aligned} \quad (4)$$

2.4. Solution method

The commercial CFD package FLUENT (v.6.3.26) is employed for numerical simulation of turbulent flow in the turbulence promoter-inserted tube. The geometry modeling of rod baffle and disc baffle is created using GAMBIT. The geometry modeling of helical baffle is created using Pro/Engineer package. Mesh generation for three cases is implemented using GAMBIT. The assumption of non-permeable wall is adopted and the no-slip boundary condition is applied in this study, which is widely employed in literature.

The pressure-velocity coupling is handled via the SIMPLE algorithm, and the convective terms are discretized by a second-order upwind scheme. The enhanced wall treatment is adopted when using RNG $k-\epsilon$ model for CFD simulation. A grid size small enough is chosen based on the comparison of results from a succession of finer meshes to ensure that the simulation results are independent of the grid size.

The scaled residuals are set to a criterion of at least 10^{-5} for the continuity, momentum and $k-\epsilon$ variables to ensure the solution convergence. In addition, the variation of pressure magnitude at the tube inlet (defined as velocity-inlet boundary condition) and variation of velocity magnitude at the tube outlet (defined as pressure-outlet boundary condition) are monitored as an indicator of solution convergence at the same time.

3. Results and discussion

In order to investigate the effects of turbulence promoter configurations on flow patterns which plays an important role in membrane filtration performance, the turbulent flow in tubular channel inserted with turbulence promoter was numerically simulated under the same condition, that is, the inlet velocity of 0.5 m/s ($Re = \sim 7,500$ for the empty tube) and outlet pressure of 50 kPa.

3.1. Velocity vectors

Fig. 2 shows the velocity vectors of fluid flow in the tubular channel centrally inserted with a rod baffle. As illustrated

in Fig. 2(a), when the fluid flows around the rod baffle, the crossflow velocity is largely increased due to the constriction of cross-sectional area. At an inlet velocity of 0.5 m/s, the fluid velocity significantly increases to ~ 1.0 m/s in the constricted regions. Fig. 2(b) presents the flow patterns of the cross-sectional tube in axial direction. The behavior of fluid flow around a rod baffle can be clearly observed from this figure. The vortex formation can be observed at the end of turbulence promoter. Fig. 2(c) shows the velocity vectors of the cross-sectional tube in radial direction ($z = 0.035$ m). The behavior of annular flow can be clearly observed from this figure. The significant increase of flow velocity within the radial clearance gap can also be observed from this figure. It tends to promote the turbulence level of fluid flow in the membrane channel, which can effectively diminish the particle deposition on the membrane surface.

Fig. 3 displays the velocity vectors of fluid flow in tubular channel centrally inserted with disc baffles. As illustrated in Fig. 3(a), when the fluid is forced to flow around an array of disc baffles, the flow velocity in the neighborhood of channel wall sharply increases, which tends to effectively sweep the membrane surface, thereby diminishing the particle deposition on the membrane surface. The presence of disc baffle causes the distortion of stream lines, giving rise to the eddy formation on the downstream side of disc baffles, as illustrated in Fig. 3(b). The reason for eddy formation can be explained as follows. When the fluid flows around disc baffle, it creates a

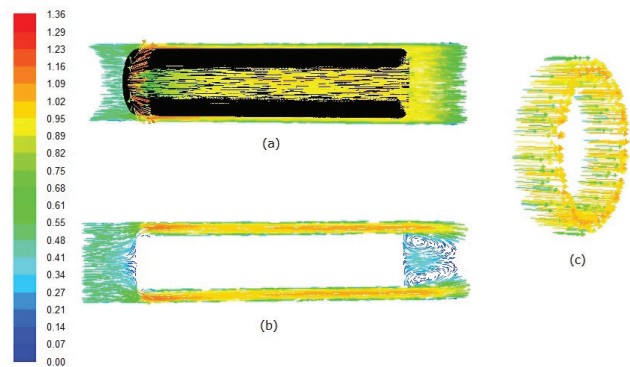


Fig. 2. Velocity vectors of fluid flow in the tube inserted with a rod baffle. (a) tube cross-section, (b) Y-Z section and (c) Y-X section.

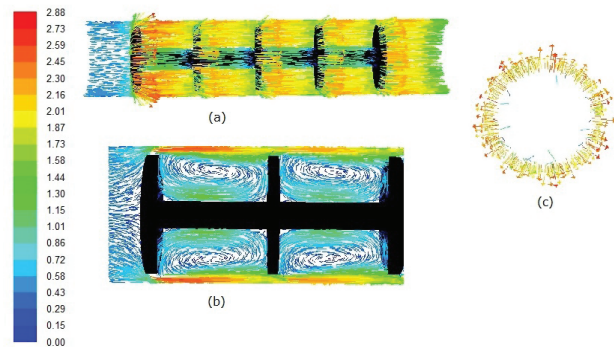


Fig. 3. Velocity vectors of fluid flow in the tube inserted with a disc baffle. (a) tube cross-section, (b) Y-Z section and (c) Y-X section.

space devoid of downstream-flowing fluid. Fluid behind disc baffle flows into the space void creating a swirling of fluid, followed by a short reverse flow of fluid behind the baffle flowing upstream. The eddy motion has a two-sided effect on the membrane performance. On one hand, eddy motion can sweep the membrane surface due to its excellent eddy mixing, which can effectively disrupt the development of concentration boundary layer in the inter-baffle regions. The eddy mixing action also can facilitate the back transfer of rejected particles away from the membrane surface to the bulk flow, which is responsible for the diminished particle deposition. On the other hand, it also increases the pressure drop due to energy dissipation of turbulent flow, which will be discussed in the following sections. Fig. 3(c) shows the velocity vectors at the position where the disc baffle is located ($z = 0.01$ m), in which the annular flow can be clearly observed.

Fig. 4 shows the velocity vectors of fluid flow in tubular channel centrally inserted with a helical baffle. As illustrated in Fig. 4(a), the fluid flow in the channel is mainly divided into two portions, that is, the helical flow within the helical groove and the axial flow through the radial clearance gap. As the small portion of fluid flow, the axial flow with a relatively higher velocity can disrupt the development of concentration boundary layer on membrane surfaces. As the bulk portion of fluid flow, the helical flow can enhance the convective mixing of feed solution. Fig. 4(b) shows the formation of secondary flow within the helical groove. It has been widely accepted that the secondary flow introduces the unsteadiness into the bulk flow and increases the convective mixing of feed solution, thereby improving the membrane performance [31,32]. Fig. 4(c) shows the rotational flow pattern, which can increase the scouring effect on the tube wall, thereby diminishing the particle deposition on the membrane surface.

3.2. Velocity contours

Fig. 5 shows the velocity contours of fluid flow in the tubular channel centrally inserted with a rod baffle. The presence of a rod baffle produces a distinct constriction of tube cross-section for fluid flow, as illustrated in Fig. 5(c). As a result, the fluid flow in the whole tube keeps relatively higher velocity, as illustrated in Fig. 5(a). At the inlet velocity of 0.5 m/s, the crossflow velocity of fluid within the radial clearance gap sharply increases to about 1.0 m/s. As illustrated in

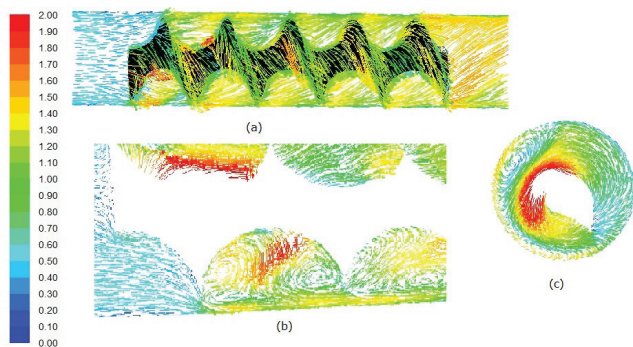


Fig. 4. Velocity vectors of fluid flow in the tube inserted with a helical baffle. (a) tube cross-section, (b) Y-Z section and (c) Y-X section.

Fig. 5(b), the absence of dead zone or stagnant region where the particles in the feed are readily deposited on the membrane surface, can be observed in the vicinity of channel wall. It is a desirable hydrodynamic feature to avoid the membrane fouling.

Fig. 6 displays the velocity contours of fluid flow in the tubular channel centrally inserted with a disc baffle. The insertion of a disc baffle causes a distinct constriction (Fig. 6(c)) followed by a long enlargement of cross-section for fluid flow, as illustrated in Fig. 6(a). As a result, flow velocity sharply speeds up at the position where the disc is located and then gradually slows down at the baffle interval. Fig. 6(b) shows that the fluid in the neighborhood of channel wall keeps a relatively higher velocity. It is desirable for membrane modules to alleviate the membrane fouling.

Fig. 7 exhibits the velocity contours of fluid flow in the tubular channel centrally inserted with a helical baffle. As illustrated in Fig. 7(a), the presence of a helical baffle makes the fluid within the module rotate around the baffle. As a result, the fluid flow in the whole tube keeps a relatively high velocity. Fig. 7(b) shows the absence of dead zones or stagnant regions in the vicinity of tube wall, which is desirable to alleviate the membrane fouling. Fig. 7(c) exhibits the constriction of cross-sectional area due to the presence of helical baffle.

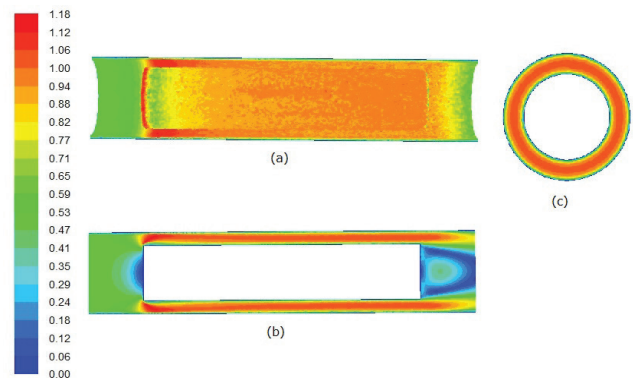


Fig. 5. Velocity contours of fluid flow in the tube inserted with a rod baffle. (a) tube cross-section, (b) Y-Z section and (c) Y-X section.

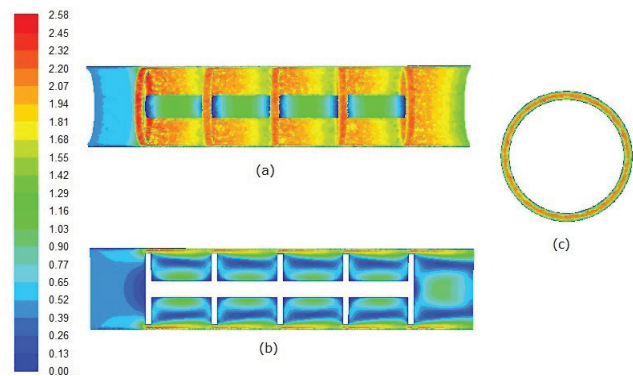


Fig. 6. Velocity contours of fluid flow in the tube inserted with a disc baffle. (a) tube cross-section, (b) Y-Z section and (c) Y-X section.

For an empty tube, a laminar flow layer exists at the wall whenever the fluid flow in the bulk stream is turbulent or laminar. Under the circumstances, the particles in the feed are prone to deposit on the membrane surface, resulting in the formation of cake layer. As to the turbulence promoter-inserted tube, the absence of laminar flow layer can be found. The presence of turbulence promoter can increase the turbulence level in the bulk fluid. It tends to alleviate the concentration polarization and membrane fouling, thereby promoting the filtration performance.

3.3. Wall velocity distributions

The filtration performance is closely related to the hydrodynamic conditions on the membrane surface. It has been widely accepted that increasing crossflow velocity can effectively reduce the particle deposition on membrane surfaces and improve the filtration performance. Fig. 8 shows the distributions of wall velocity in the turbulence promoter-inserted tube. Among three cases, the disc baffle generates the most intensive fluctuation of wall velocity, which is followed by helical baffle. Possible explanation lies in the different flow

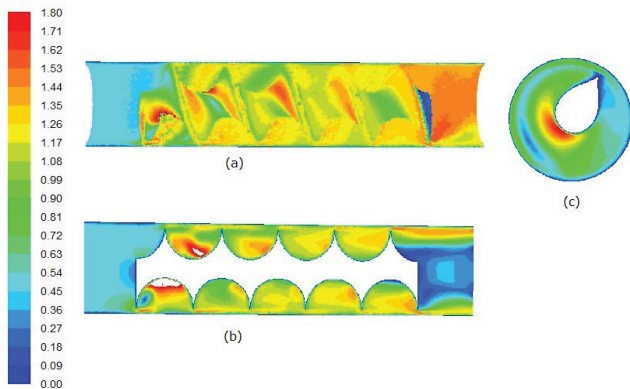


Fig. 7. Velocity contours of fluid flow in the tube inserted with a helical baffle. (a) tube cross-section, (b) Y-Z section and (c) Y-X section.

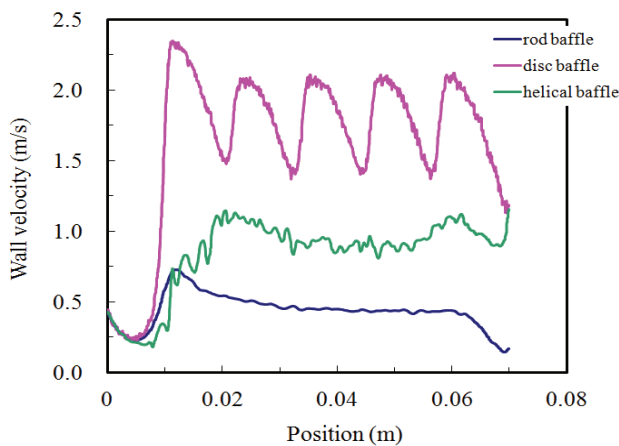


Fig. 8. Wall velocity of fluid flow in turbulence promoter-inserted tube.

patterns that turbulence promoter encourages within the tubular channel. In comparison with rod baffle, helical baffle produces the much more intense velocity fluctuation, which is attributed to the rotational flow patterns and secondary vortices generated by the helical configuration. In contrast to disc baffle, helical baffle generates the less intensive velocity fluctuation owing to its streamline shape of geometric configuration.

3.4. Distributions of wall shear stress

Normally, the use of turbulence promoter increases the crossflow velocity, leading to an increase in the wall shear stress which is responsible for the improved membrane filtration performance. The distribution of wall shear stress in the turbulence promoter-inserted tube is illustrated in Fig. 9. For each baffle case, the fluctuation tendency of wall shear stress is similar to that of wall velocity. The disc baffle generates the most intensive fluctuation of wall shear stress, followed by helical baffle and rod baffle. As a whole, the average value of wall shear stress is 37.1, 16.9 and 8.2 Pa for disc baffle, helical baffle and rod baffle, respectively. Increasing wall shear stress can promote the back transfer of deposited particle away from membrane surfaces due to the shear-induced diffusion, thereby diminishing the particle deposition on membrane surfaces. Therefore, high wall shear stress is responsible for the improved membrane performance. From the point of view of wall shear stress, it can be concluded that disc baffle can achieve the highest membrane filtration flux among three baffle cases.

3.5. Turbulence characteristics

The use of turbulence promoter in the channel not only increases the crossflow velocity but also produces the turbulence of fluid flow. Fig. 10 shows the distributions of turbulence intensity along the tubular channel inserted with different baffles. As an index of turbulent level of fluid flow, the turbulence intensity (I) is defined as a ratio of the random velocity to the time-averaged velocity.

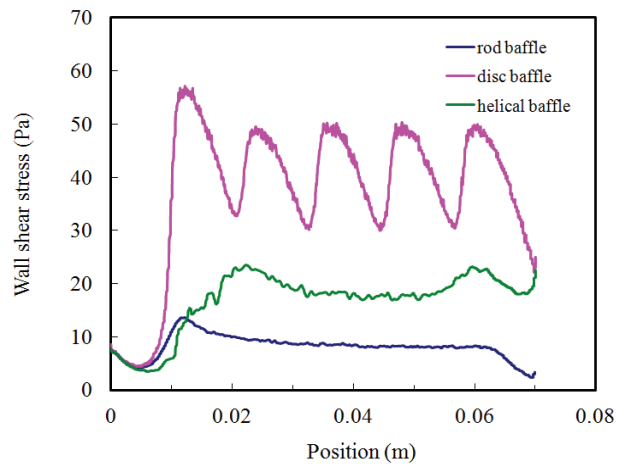


Fig. 9. Wall shear stress of fluid flow in turbulence promoter-inserted tube.

$$I = \frac{u'}{\bar{u}} \times 100\% \quad (5)$$

where u' and \bar{u} are the random velocity and time-averaged velocity, respectively.

Compared with rod baffle, helical baffle produces the considerably higher turbulence level of fluid flow due to the frequent change in flow direction. In contrast to helical baffle, disc baffle generates the much higher turbulence intensity owing to the fluctuation of velocity fields and the eddy formation. The turbulence is known to disturb the concentration polarization mechanism to a great extent by reducing the build-up of particles on membrane surfaces. From this point of view, it indicates that disc baffle achieves the best membrane performance among three baffle cases.

3.6. Pressure drop

Fig. 11 shows the distributions of static pressure along the turbulence promoter-inserted channel. From this figure, the axial pressure drop along the channel, that is, pressure difference between tube inlet and outlet can be obtained. At an inlet velocity of 0.5 m/s, the pressure drop along the baffle-filled channel is about 10.35, 3.71 and 0.67 kPa for the disc baffle, helical baffle and rod baffle, respectively. For the helical baffle, the high pressure drop is mainly attributed to the frequent change in flow direction and secondary flow within the helical configuration. As to the disc baffle, the intensive velocity fluctuation and eddy formation are responsible for the increased pressure drop along the baffled channel. The high pressure drop along the channel indicates the increased energy costs of membrane modules due to the turbulent energy dissipation.

3.7. Microfiltration experiment

For a traditional membrane system, high wall shear stress is responsible for the improved filtration performance because it can effectively disturb the build-up of a cake layer

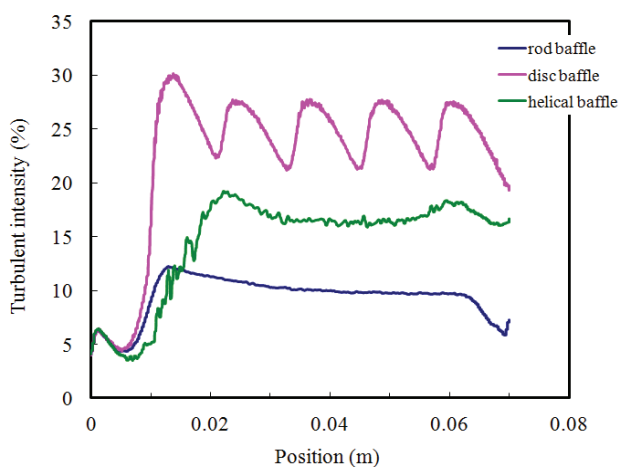


Fig. 10. Turbulence intensity of fluid flow in turbulence promoter-inserted tube.

deposited on the membrane surface. As to the baffle-filled membrane system, filtration performance is closely related to the hydrodynamic conditions on the membrane surface.

In order to validate CFD simulation, crossflow micro-filtration of CaCO_3 suspension ($C = 1.0 \text{ g/L}$) was conducted at an inlet velocity of 0.5 m/s and trans-membrane pressure of 0.5 bar. It can be observed from Fig. 12 that the baffled membrane systems achieve higher filtration flux than the traditional system, with an increase by 17% (rod baffle), 28% (helical baffle) and 40% (disc baffle) respectively. The flux enhancement by the baffles can be attributed to the intense fluctuations of local velocity fields, high wall shear stress and eddy formation, which can greatly disrupt the development of boundary layer and reduce the cake deposition on the membrane surface. Among three baffle cases, the disc baffle achieves the highest permeate flux due to the excellent turbulence-promoting action, which is consistent with the prediction of CFD simulation.

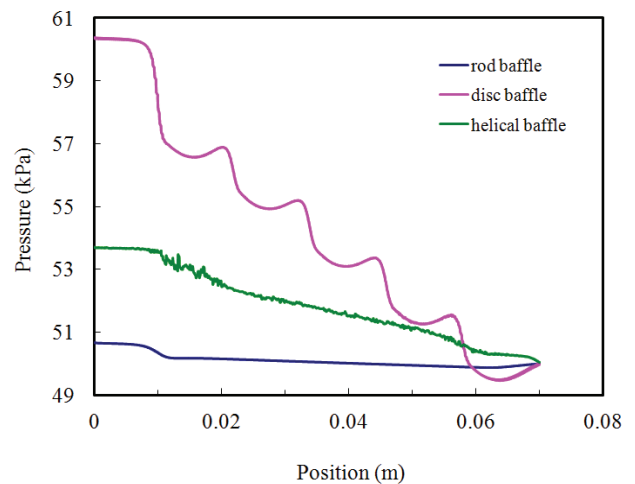


Fig. 11. Distributions of static pressure in turbulence promoter-inserted tube.

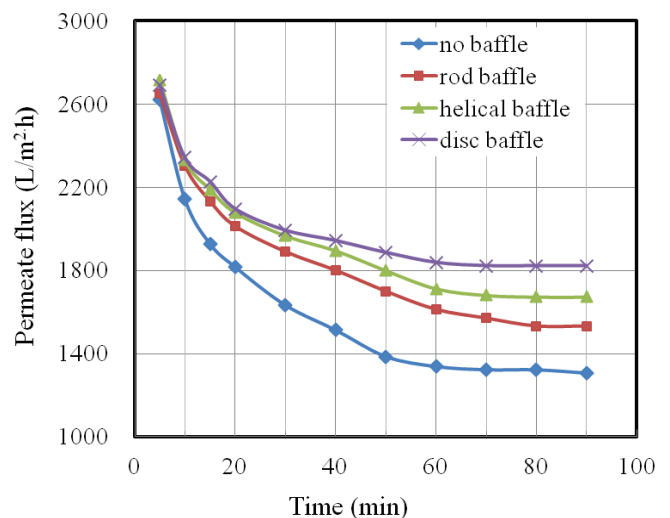


Fig. 12. Effects of baffle configuration on the membrane permeate flux.

As mentioned in Section 3.6, the pressure drop along the channel is increased due to the presence of turbulence promoter. Therefore the energy costs of membrane modules should be taken into account when the turbulence promoter is utilized to improve filtration performance. The most important parameter from an economic point of view is the specific hydraulic energy consumption E_p (J/m^3), which is defined as the hydraulic power dissipated per unit volume of permeate [33,34]:

$$E_p = \frac{\Delta P \cdot Q}{v \cdot S} \quad (6)$$

where ΔP is the pressure drop along the channel (Pa), Q is the flow rate (m^3/s), v is the membrane flux (m/s) and S is the membrane area (m^2).

According to Eq. (6), the specific hydraulic energy consumption of baffled membrane system was calculated, which is $42.2 \text{ kJ}/\text{m}^3$ (rod baffle), $214.7 \text{ kJ}/\text{m}^3$ (helical baffle) and $549.3 \text{ kJ}/\text{m}^3$ (disc baffle), respectively. Although the disc baffle achieves the best membrane performance (increased by 40%), the specific hydraulic energy consumption is the highest among three baffle cases. It suggests that the optimization of turbulence promoter-inserted membrane system involves a trade-off between these competing effects.

4. Conclusions

The turbulent flow in tubular membrane channel centrally inserted with a turbulence promoter was numerically simulated. The effects of turbulence promoter configurations on the flow patterns, behavior and feature in tubular membrane channel were investigated through CFD simulation. The disc baffle generates a rather more complex flow field than helical baffle or rod baffle, and causes much more intense fluctuations of velocity magnitude and wall shear stress, which is favorable for the membrane filtration process. The disc baffle produces the fairly higher turbulence level of fluid flow within membrane module than helical baffle or rod baffle, which is beneficial to disrupt the development of concentration boundary layer and prevent particle deposition on the membrane surface. The disc baffle greatly intensifies the eddy mixing action, which can facilitate the back transfer of rejected particles away from membrane surfaces to the bulk flow. CFD simulation indicates that the disc baffle can achieve a better membrane performance than helical baffle or rod baffle, which is validated by the microfiltration experiment. However, as a price, the pressure drop along the baffle-filled tube is increased due to the frequent changes in flow direction and high turbulent flow dissipation, indicating the increased energy costs of membrane module. Therefore, the optimization of baffled membrane system involves a trade-off between these competing effects.

Symbols

ρ	—	Density, kg/m^3
u	—	Velocity, m/s
t	—	Time, s
u_i	—	i component of velocity, m/s

u_j	—	j component of velocity, m/s
x_i	—	i coordinate
x_j	—	j coordinate
μ	—	Viscosity, Pa s
p	—	Pressure, Pa
μ_t	—	Turbulent viscosity, Pa s
δ_{ij}	—	Kronecker sign
k	—	Turbulent kinetic energy, m^2/s^2
ε	—	Turbulence dissipation rate, m^2/s^3
C_μ	—	Constant related to viscosity
$C_{1\varepsilon}$	—	Constant related to modulus 1 of turbulence dissipation rate
$C_{2\varepsilon}$	—	Constant related to modulus 2 of turbulence dissipation rate
σ_k	—	Coefficient related to turbulent kinetic energy
σ_ε	—	Coefficient related to turbulence dissipation rate

References

- [1] S. Wang, C. Liu, Q. Li, Fouling of microfiltration membranes by organic polymer coagulants and flocculants: controlling factors and mechanisms, *Water Res.*, 45 (2011) 357–365.
- [2] Y. Liu, G. He, B. Li, Z. Hu, J. Ju, A comparison of cake properties in traditional and turbulence promoter assisted microfiltration of particulate suspensions, *Water Res.*, 46 (2012) 2535.
- [3] S. Lee, P.K. Park, J.H. Kim, K.M. Yeon, C.H. Lee, Analysis of filtration characteristics in submerged microfiltration for drinking water treatment, *Water Res.*, 42 (2008) 3109–3121.
- [4] D.C. Choi, S.Y. Jung, Y.J. Won, J.H. Jang, J. Lee, H.R. Chae, K.H. Ahn, S. Lee, P.K. Park, C.H. Lee, Three-dimensional hydraulic modeling of particle deposition on the patterned isopore membrane in crossflow microfiltration, *J. Membr. Sci.*, 492 (2015) 156–163.
- [5] M.A. Monfared, N. Kasiri, A. Salahi, T. Mohammadi, Modeling ultrafiltration of gelatin–water suspension by computational fluid dynamics, *Chem. Eng. Res. Des.*, 90 (2012) 1098–1104.
- [6] C. Completo, V. Semiao, V. Geraldes, Efficient CFD-based method for designing cross-flow nanofiltration small devices, *J. Membr. Sci.*, 500 (2016) 190–202.
- [7] S.S. Bucs, R.V. Linares, J.O. Marston, A.I. Radu, J.S. Vrouwenvelder, C. Picioreanu, Experimental and numerical characterization of the water flow in spacer-filled channels of spiral-wound membranes, *Water Res.*, 87 (2015) 299–310.
- [8] M. Rezakazemi, M. Shahverdi, S. Shirazian, T. Mohammadi, A. Pak, CFD simulation of water removal from water/ethylene glycol mixtures by pervaporation, *Chem. Eng. J.*, 168 (2011) 60–67.
- [9] H. Li, U. Schyggulla, J. Hoffmann, P. Niehoff, K. Haas-Santo, R. Dittmeyer, Experimental and modeling study of gas transport through composite ceramic membranes, *Chem. Eng. Sci.*, 108 (2014) 94–102.
- [10] X. Liu, W. Yuan, T.D. Waite, G. Leslie, Numerical simulation of bubble induced shear in membrane bioreactors: effects of mixed liquor rheology and membrane configuration, *Water Res.*, 75 (2015) 131–145.
- [11] Y. Zhang, Y. Peng, S. Ji, S. Wang, Numerical simulation of 3D hollow-fiber vacuum membrane distillation by computational fluid dynamics, *Chem. Eng. Sci.*, 152 (2016) 172–185.
- [12] R. Kieffer, C. Charcosset, F. Puel, D. Mangin, Numerical simulation of mass transfer in a liquid–liquid membrane contactor for laminar flow conditions, *Comput. Chem. Eng.*, 32 (2008) 1325–1333.
- [13] S.S. Hla, L.D. Morpeth, M.D. Dolan, Modelling and experimental studies of a water-gas shift catalytic membrane reactor, *Chem. Eng. J.*, 276 (2015) 289–302.
- [14] Y. Liu, G. He, L. Ding, H. Dou, J. Ju, B. Li, Experimental and CFD studies on the performance of microfiltration enhanced by a turbulence promoter, *Chin. J. Chem. Eng.*, 20 (2012) 617–624.

- [15] C.P. Koutsou, S.G. Yiantsios, A.J. Karabelas, Numerical simulation of the flow in a plane-channel containing a periodic array of cylindrical turbulence promoters, *J. Membr. Sci.*, 231 (2004) 81–90.
- [16] Y. Liu, G. He, X. Liu, G. Xiao, B. Li, CFD simulations of turbulent flow in baffle-filled membrane tubes, *Sep. Purif. Technol.*, 67 (2009) 14–20.
- [17] Z. Cao, D.E. Wiley, A.G. Fane, CFD simulations of net-type turbulence promoters in a narrow channel, *J. Membr. Sci.*, 185 (2001) 157–176.
- [18] M. Shakaib, S.M.F. Hasani, M. Mahmood, Study on the effects of spacer geometry in membrane feed channels using three-dimensional computational flow modeling, *J. Membr. Sci.*, 297 (2007) 74–89.
- [19] Y. Liu, X. Luo, G. He, Y. Yu, J. Guo, Y. Gong, H. Zhang, CFD study on the effect of baffle arrangements on flow patterns in tubular membrane channel, *Desal. Wat. Treat.*, 75 (2017) 10–17.
- [20] J.L.C. Santos, V. Geraldes, S. Velizarov, J.G. Crespo, Investigation of flow patterns and mass transfer in membrane module channels filled with flow-aligned spacers using computational fluid dynamics (CFD), *J. Membr. Sci.*, 305 (2007) 103–117.
- [21] A.L. Ahmad, A. Mariadas, Baffled microfiltration membrane and its fouling control for feed water of desalination, *Desalination*, 168 (2004) 223–230.
- [22] D.M. Krstic, M.N. Tekic, M.D. Caric, S.D. Milanovic, Kenics static mixer as turbulence promoter in cross-flow microfiltration of skim milk, *Sep. Sci. Technol.*, 38 (2003) 1549–1560.
- [23] H.M. Yeh, Y.F. Chen, Modified analysis of permeate flux for ultrafiltration in a solid-rod tubular membrane, *J. Membr. Sci.*, 251 (2005) 255–261.
- [24] B.B. Gupta, J.A. Howell, D. Wu, R.W. Field, A helical baffle for cross-flow microfiltration, *J. Membr. Sci.*, 102 (1995) 31–42.
- [25] Y. Liu, G. He, M. Tan, F. Nie, B. Li, Artificial neural network model for turbulence promoter-assisted crossflow microfiltration of particulate suspensions, *Desalination*, 338 (2014) 57–64.
- [26] S. Popović, M.N. Tekić, Twisted tapes as turbulence promoters in the microfiltration of milk, *J. Membr. Sci.*, 384 (2011) 97–106.
- [27] A. Jokić, Z. Zavargo, Z. Šereš, M. Tekić, The effect of turbulence promoter on cross-flow microfiltration of yeast suspensions: a response surface methodology approach, *J. Membr. Sci.*, 350 (2010) 269–278.
- [28] H.G. Gomaa, S. Rao, M.A. Taweel, Flux enhancement using oscillatory motion and turbulence promoters, *J. Membr. Sci.*, 381 (2011) 64–73.
- [29] J. Liu, Z. Liu, F. Liu, W. Wei, Z. Li, X. Wang, D. Chao, X. Xu, The application of saw-tooth promoter for flat sheet membrane filtration, *Desalination*, 359 (2015) 149–155.
- [30] J. Liu, Z. Liu, X. Xu, F. Liu, Saw-tooth spacer for membrane filtration: hydrodynamic investigation by PIV and filtration experiment validation, *Chem. Eng. Process. Process Intens.*, 91 (2015) 23–34.
- [31] B.J. Bellhouse, G. Costigan, K. Abhinava, A. Merry, The performance of helical screw-thread inserts in tubular membranes, *Sep. Purif. Technol.*, 22–23 (2001) 89–113.
- [32] H.R. Millward, B.J. Bellhouse, G. Walker, Screw-thread flow promoters: an experimental study of ultrafiltration and microfiltration performance, *J. Membr. Sci.*, 106 (1995) 269–279.
- [33] T.Y. Chiu, A.E. James, Effects of axial baffles in non-circular multi-channel ceramic membranes using organic feed, *Sep. Purif. Technol.*, 51 (2006) 233–239.
- [34] N. Xu, W. Xing, N. Xu, J. Shi, Study on ceramic membrane bioreactor with turbulence promoter, *Sep. Purif. Technol.*, 32 (2003) 403–410.